Journal of Power Sources 189 (2009) 665–668

Contents lists available at ScienceDirect

Journal of Power Sources

journal homepage: www.elsevier.com/locate/jpowsour

Short communication

Micro- and macroscopic magnetism in Li_xNiO_2

K. Mukai[a,*], J. Sugiyama[a], Y. Ikedo[a], P.L. Russo[b], D. Andreica[c,d], A. Amato[c], K. Ariyoshi[e], T. Ohzuku[e]

[a] Toyota Central Research and Development Laboratories, Inc., Yokomichi 41-1, Nagakute, Aichi 480-1192, Japan
[b] TRIUMF, 4004 Wesbrook Mall, Vancouver, BC V6T 2A3, Canada
[c] Paul Scherrer Institut, Villigen CH-5232, Switzerland
[d] Faculty of Physics, Babes-Bolyai University, 400084 Cluj-Napoca, Romania
[e] Department of Applied Chemistry, Osaka City University, Osaka 558-8585, Japan

ARTICLE INFO

Article history:
Received 31 July 2008
Accepted 10 September 2008
Available online 27 September 2008

Keywords:
Lithium-ion battery
Lithium nickel oxide
Magnetism
Muon-spin rotation/relaxation (μ^+SR)

ABSTRACT

Both macro- and microscopic magnetic nature of Li_xNiO_2 ($0.1 \le x \le 1$) were studied by susceptibility (χ) and muon-spin rotation and relaxation (μ^+SR) measurements in order to understand the change in magnetism of Li_xNiO_2 with x. The χ measurements showed the presence of spin-glass-like freezing at $T_f \sim 11$ K for the samples in the whole x range measured. This implies that the macroscopic magnetism is not sensitive to x, although the crystal structure and average oxidation state of the Ni ions of Li_xNiO_2 alter as a function of x. On the other hand, the microscopic magnetism of Li_xNiO_2 is found to be quite different from the macroscopic one. That is, a static antiferromagnetic ordered phase appears at low T for the samples with $0.6 \le x \le 1$, while a spin-glass-like disordered phase presents for the $0.25 \le x \le 0.5$ samples below 10 K.

1. Introduction

A nickel dioxide $LiNiO_2$ has a layered structure, in which the Li plane is sandwiched by the two adjacent NiO_2 planes. Furthermore, the NiO_2 planes are formed by the network of edge-sharing NiO_6 octahedra, resulting in a rigid framework of a layered structure. Since Li^+ ions are easily extracted and/or inserted by an electrochemical reaction, $LiNiO_2$ has been extensively studied as a positive electrode material of lithium-ion batteries [1,2]. In the $LiNiO_2$lattice, the Ni^{3+}ions are in a low-spin state with $S = 1/2$ ($t_{2g}^6 e_g^1$) [3], due to a strong crystalline electric field of the NiO_6 octahedral coordination. This electron configuration is naturally expected to induce a cooperative Jahn–Teller (JT) distortion for $LiNiO_2$, as in the case for $NaNiO_2$[4]. Indeed, an EXAFS study on $LiNiO_2$ showed the presence of local distortion of the NiO_6 octahedra; that is, among the six Ni–O bonds, two bond lengths are longer than that for the rest four [5]. However, in contrast to $NaNiO_2$, a cooperative JT distortion has never been observed for $LiNiO_2$ so far.

On the other hand, the crystal structure of the Li-deintercalated Li_xNiO_2 phase is known to depend on x at ambient temperature (T); as x decreases from 1, a rhombohedral ($R\bar{3}m$) phase is stable down to $x = 0.75$, whereas a monoclinic ($C2/m$) phase in the x range between 0.75 and ~ 0.45. Then, with further lowering x, a rhombohedral phase appears again with $0.25 \le x \le 0.45$, and finally two rhombohedral phases coexist below $x < 0.25$ [2]. In order to explain the phase transition between $R\bar{3}m$ and $C2/m$ phase with $0.45 \sim x \le 0.75$, two hypotheses were proposed; one is due to a cooperative JT distortion of Ni^{3+} ions [2] and the other is due to ordering of Li^+ ions [6]. However, the driving force of this phase transition is currently not fully understood.

In this paper, we report susceptibility (χ) and muon-spin rotation and relaxation (μ^+SR) study on Li_xNiO_2in order to understand the reaction scheme of Li_xNiO_2, because magnetic nature is expected to be very sensitive to the crystal structure and oxidation state of the Ni ions. Here, μ^+SR provides a local magnetic information and is one of the powerful techniques to detect both static and dynamic internal magnetic fields from 0.1 Oe to 100 kOe caused by nuclear- and electronic-magnetic moments [7,8].

2. Experimental

Three different samples of $LiNiO_2$ (Lot A, B, and C) were prepared using the following solid state reaction. The reaction mixtures of $LiNO_3$ ($Li(OH)\cdot H_2O$ for Lot B) and $NiCO_3$ (NiO for Lot B) were pressed into a pellet of 23 mm diameter and ~ 5 mm thickness. Then the pressed pellet was heated at 650 °C in oxygen flow for 12 h. The obtained powder was crushed, repressed into a pellet, and then fired at 750 °C in oxygen flow for 12 h. According to an induction coupled plasma (ICP) atomic emission spectral (AES) analysis

* Corresponding author. Tel.: +81 561 71 7698; fax: +81 561 63 6137.
E-mail address: e1089@mosk.tytlabs.co.jp (K. Mukai).

0378-7753/$ – see front matter © 2008 Elsevier B.V. All rights reserved.
doi:10.1016/j.jpowsour.2008.09.069

(CIROS 120, Rigaku Co. Ltd., Japan), the Li/Ni ratios for Lot A, B, and C were determined to be 1.01, 0.97, 0.99, respectively. The final products were characterized by a powder XRD (RINT-2200, Rigaku Co. Ltd., Japan) analysis and an electrochemical measurement.

χ measurements were carried out using a superconducting quantum interference device (SQUID) magnetometer (MPMS, Quantum Design) in the T range between 5 and 400 K under magnetic field $H \leq 10$ kOe. μ^+SR experiments were performed at the Paul Scherrer Institut, Switzerland. The powder samples were pressed into a disk of about 15 mm diameter and 1 mm thickness, and subsequently placed into a fork-type low background sample holder. The experimental setup and technique were described in elsewhere [7,8].

The Li_xNiO_2samples for the χ and μ^+SR measurements were prepared by an electrochemical reaction in non-aqueous Li cells. The electrolyte was 1 M $LiPF_6$ dissolved in ethylene carbonate (EC)/diethyl carbonate (DMC) (3/7 volume ratio) solution. In order to avoid the χ and μ^+SR signals from conducting additives and a binder, the electrodes were entirely made from $LiNiO_2$ powder. The Li_xNiO_2 powders were removed from the cells in a He filled glovebox just before μ^+SR measurements. In order to know the possible change in the Li_xNiO_2 samples during μ^+SR measurement, the samples were returned to the cells after the measurement to check its open circuit voltage vs. Li^+/Li. The above procedure is essentially the same to that of our recent μ^+SR work on Li_xCoO_2[9,10].

3. Results and discussion

In an ideal $LiNiO_2$lattice with a space group of $R\bar{3}m$, Li ions occupy 3*b* site and Ni ions 3*a* site, respectively, in the cubic close-packed oxygen array. However, the ideal stoichiometric $LiNiO_2$ has been never prepared so far. Since the obtained samples always include excess Ni ions at 3*b* site, their ionic distribution is represented by $(Li_{1-y}Ni_y)_{3b}[Ni_{1-y}]_{3a}O_2$[11]. The Ni ions at 3*b* site induce an additional ferromagnetic (FM) interaction between the adjacent two NiO_2planes, whether the Ni_{3b}–Ni_{3a} coupling is antiferromagnetic (AF) or FM [12]. As a result, it is well known that the magnetic nature of $LiNiO_2$ significantly depends on y [11]. We, therefore, firstly estimated y for the present $LiNiO_2$ samples by XRD and electrochemical measurements. The $LiNiO_2$ samples with Lot A, B, and C were identified as a layered structure with a space group of $R\bar{3}m$. The lattice parameters in the hexagonal setting were calculated to be $a_h = 2.879$ Å, $c_h = 14.199$ Å for Lot A, $a_h = 2.878$ Å, $c_h = 14.193$ Å for Lot B, and $a_h = 2.878$ Å, $c_h = 14.198$ Å for Lot C, respectively. According to the ratio between the intensity of an XRD peak I(0 0 3) and I (1 0 4) and the ICP-AES analysis, y for the three samples is roughly estimated below 0.03 [2].

Fig. 1(a) shows the charge and discharge (C/D) curves of $Li/LiNiO_2$ cells for the three samples operated with a rate of 0.17 mA cm^{-2} at 25 °C. The C/D curves for all the samples exhibit three plateaus at ~ 3.6 V, 4.0 V, and 4.2 V. The rechargeable capacities in the voltage range between 2.5 and 4.2 V are found to be ~ 166 mAh g^{-1}, 175 mAh g^{-1}, and 181 mAh g^{-1} for Lot A, B, and C, respectively. The difference in the rechargeable capacities between lots is probably caused by the fact that the upper cutoff voltage is very close to the third plateau at ~ 4.2 V. The structural and electrochemical properties for the present samples are hence consistent with the previous result [2].

The charge curves of the cells for the χ and μ^+SR experiments are shown in Fig. 1(b). Although the amount of the $LiNiO_2$powder in the cell is 0.1 g for the χ and 0.2 g for μ^+SR measurements, the cell was charged slowly with a rate of ~ 0.057 mA cm^{-2} (= 0.5 mA g^{-1}), due to the absence of conducting additives and a binder. Since the charge curves for the all samples trace the curve for the conventional electrode mix, the Li-deintercalated reaction is found to be successfully achieved for the all Li_xNiO_2 samples. After the χ and μ^+SR measurements, the Li/Ni ratio was determined by the ICP-AES analysis. Note that the ICP-AES result is good agreement with the result of an electrochemical reaction (EC) (see Fig. 1(b)). Here, the Li/Ni ratio (EC) was estimated by the comparison between the observed charge capacity and theoretical capacity (274.5 mAh g^{-1}), assuming one-electron transfer per formula weight of $LiNiO_2$. In this paper, we use the Li/Ni ratio determined by the ICP-AES analysis. Fig. 2 shows the T dependence of χ in zero field-cooling (ZFC) and field-cooling (FC) mode with $H = 100$ Oe for the samples with (a) $x = 1$ (Lot A, B, and C), (b) $x = 0.67$ (Lot B and C), (c) $x = 0.5$ (Lot B), and (d) $x = 0.06$ (Lot A and B). For the three $x = 1$ samples, the $\chi(T)$ curve increases rapidly with decreasing T down to ~ 20 K, and then exhibits a sharp maximum (cusp) around 11 K. The cusp at 11 K is believed to be attributed to the spin-glass-like freezing (T_f) [13]. Although the three samples show the magnetic anomaly at 11 K, the $\chi_{ZFC}(T)$ curve for Lot A (Lot B) starts to deviate from $\chi_{FC}(T)$ curve below 50 K (40 K), whereas there is no difference between the two curves for Lot C above 11 K. Since the weak transverse field (wTF-) μ^+SR experiment indicates a paramagnetic nature for the three $x = 1$ samples down to ~ 20 K (described later), the difference between the $\chi_{ZFC}(T)$ and $\chi_{FC}(T)$ curve below 50 K or 40 K is not due to a formation of magnetic order.

Surprisingly, the cusp is also observed for all the samples with $x < 1$. According to the XRD analysis at ambient T, the $x = 0.67$

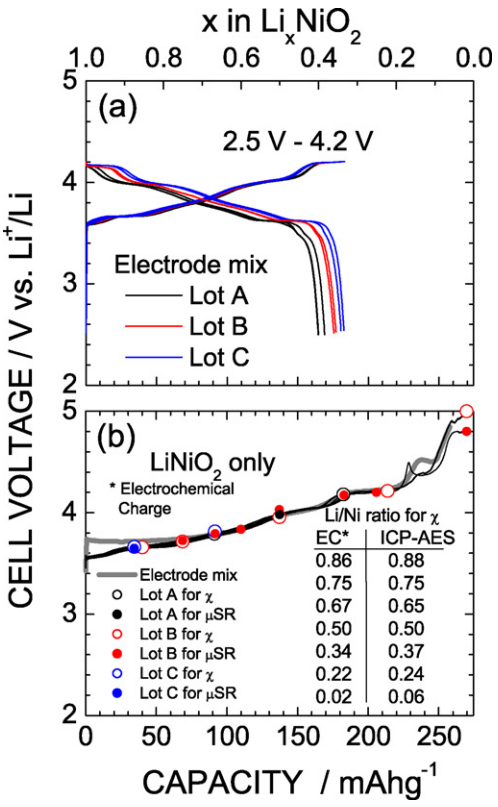

Fig. 1. The charge and discharge curves (C/D) of $Li/LiNiO_2$ cells for the samples with Lot A, B, and C: (a) the C/D curves of the cells using the conventional electrode mix, which consists of 88 wt% $LiNiO_2$, 6 wt% conductive carbon, and 6 wt% binder and (b) the charge curves of the cells for the samples of the χ and μ^+SR measurements. In order to avoid the signals from other components, the electrodes for χ and μ^+SR experiments were entirely made from $LiNiO_2$ powder. The applied current density of the cells for (a) and (b) was 0.17 and 0.057 mA cm^{-2}, respectively. The Li/Ni ratios in the Li_xNiO_2 samples for χ (open circles) and μ^+SR (closed circles) were determined by ICP-AES analysis after the measurements.

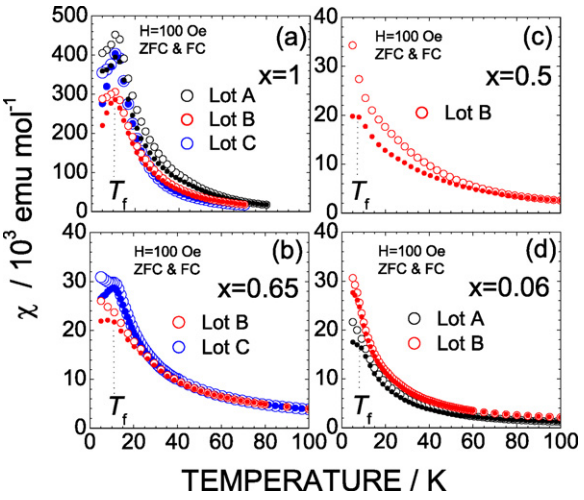

Fig. 2. Temperature dependence of χ in zero field-cooling (ZFC) and field-cooling (FC) mode with $H = 100$ Oe for the samples with (a) $x = 1$, (b) $x = 0.67$, (c) $x = 0.5$, and (d) $x = 0.06$. Here, open circles represent the data obtained in FC mode, while closed circles in ZFC mode.

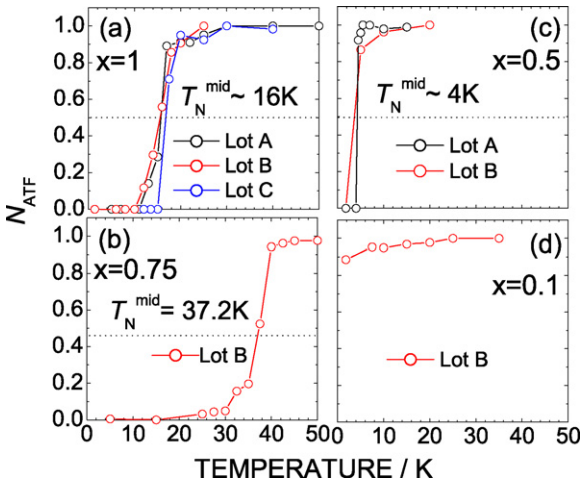

Fig. 3. Temperature dependence of the normalized wTF asymmetry [$N_{A_{TF}} = A_{TF}/A_{TF,max}$] for the Li_xNiO_2 samples with (a) $x = 1$, (b) $x = 0.75$, (c) $x = 0.5$, and (d) $x = 0.1$. The Li/Ni ratios for the μ^+SR samples were examined by ICP-AES analysis after the μ^+SR measurements.

(0.5) sample is assigned as the monoclinic phases with $a_m = 4.998$ Å, $b_m = 2.830$ Å, $c_m = 5.067$ Å, $\beta_m = 109.8°$ ($a_m = 4.946$ Å, $b_m = 2.814$ Å, $c_m = 5.091$ Å, $\beta_m = 109.7°$), while the $x = 0.1$ sample as the mixture of two hexagonal phases with $a_{h1} = 2.831$ Å, $c_{h1} = 14.418$ Å and $a_{h2} = 2.826$ Å, $c_{h2} = 13.288$ Å. Furthermore, the effective magnetic moment of Ni ions (μ_{eff}), which is estimated from the $\chi(T)$ curve obtained in FC mode with $H = 10$ kOe in the T range between 200 and 400 K, monotonically decreases from $\mu_{eff} = 2.07\ \mu_B$ for $x = 1$ to $\mu_{eff} = 0.70\ \mu_B$ for $x = 0.06$, as expected [14]. Nevertheless, T_f looks to be almost independent of x in the whole x range (see Fig. 2). The macroscopic magnetism, particularly, the spin-glass-like behavior of Li_xNiO_2 is, therefore, likely insensitive to x, although both the crystal structure and μ_{eff} are altered by x. As described above, μ^+SR is very sensitive to the local magnetic environment, because the muon interacts with predominantly its nearest neighbors [7,8]. It is, thus, sensitive to short-range magnetic order, which sometimes appears in frustrated systems, while both χ and neutron scattering measurements mainly detect long-range magnetic order. Here, weak (relative to the spontaneous internal fields in the ordered state) transverse field (wTF-) μ^+SR is sensitive to local magnetic order through the shift of the μ^+ spin precession frequency in the applied field and the enhanced muon-spin relaxation. On the other hand, zero field (ZF-) μ^+SR is uniquely sensitive to weak local magnetic [dis]order produced by quasi-static paramagnetic moments. In order to know the existence/absence of magnetic transitions, wTF- μ^+SR experiments were performed for the Li_xNiO_2 samples at first.

Fig. 3 shows the T dependence of the normalized wTF asymmetry ($N_{A_{TF}}$) for the Li_xNiO_2 samples with $x = 1$ (Lot A, B, and C), (b) $x = 0.75$ (Lot B), (c) $x = 0.5$ (Lot A and B), and (d) $x = 0.1$ (Lot B) in the applied magnetic field with wTF = 30 Oe. Here, $N_{A_{TF}}$, which is given by $A_{TF}(T)/A_{TF,max}$ ($A_{TF,max} \sim 0.24$), roughly corresponds to the volume fraction of paramagnetic phases in the sample. Except for the $x = 0.1$ sample, all the $N_{A_{TF}}(T)$ curve exhibit a step-like decrease from 1 to 0 below 40 K, demonstrating the existence of a sharp magnetic transition. More correctly, the transition T is determined as $T_N^{mid} = 16$ K for $x = 1$, $T_N^{mid} = 37$ K for $x = 0.75$, and $T_N^{mid} = 4$ K for $x = 0.5$, where T_N^{mid} is the temperature at which $N_{A_{TF}} = 0.5$. Since $N_{A_{TF}}$ reaches almost 0 below the vicinity of T_N^{mid}, the whole volume of the sample is found to enter into an AF phase below T_N^{mid}. On the contrary, for the $x = 0.1$ sample, $N_{A_{TF}} \sim 0.9$ even at 1.8 K. This is consistent with the fact that the majority of the Ni ions is in a 4+ state with $S = 0$ (t_{2g}^6). Among the nine Li_xNiO_2 samples with $0.06 \le x \le 1$, the $x = 0.75$ sample exhibits the highest T_N^{mid} (=37 K). We thus measured the ZF- μ^+SR spectrum for the $x = 0.75$ sample in order to investigate the nature of static magnetic order.

Fig. 4 shows the T dependence of the ZF- μ^+SR spectrum for the $x = 0.75$ sample in the time domain below 0.15 μs. As T decreases from 45 K to 1.8 K, the ZF-spectrum shows an almost time-independent behavior at 45 K, then shows a fast relaxation at 35 K, and finally a damped oscillation below 20 K. This means that the sample exhibits an AF transition from a high-T paramagnetic phase to a low-T AF-ordered phase. The fit using a damped

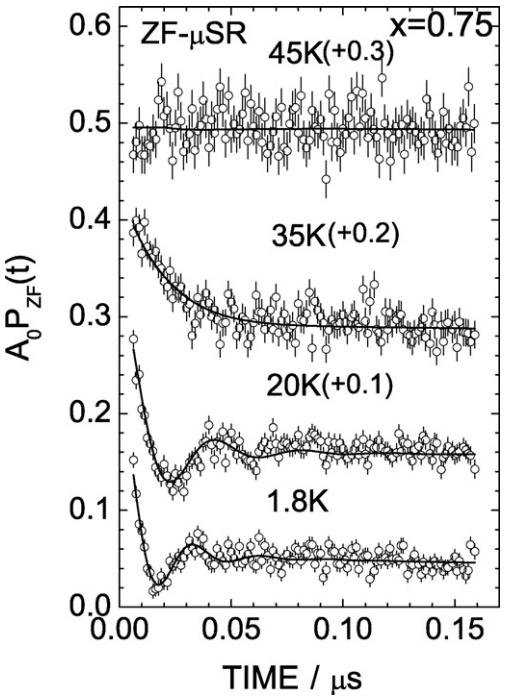

Fig. 4. Temperature dependence of the ZF- μ^+SR spectrum for the Li_xNiO_2 samples with $x = 0.75$ in the time domain below 0.15 μs. The top three spectra are each shifted upwards by 0.1 for clarity of display. Solid lines indicate the fitting results using Eq. (1).

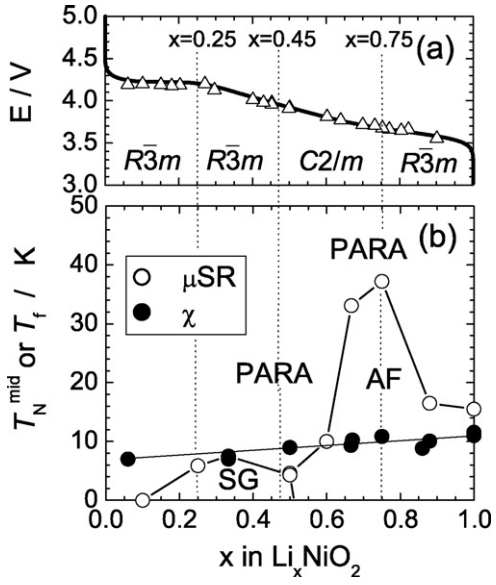

Fig. 5. The correlation between (a) the solid-state electrochemistry and (b) magnetic phase diagram of Li_xNiO_2. Data shown in triangles and solid curve in (a) were taken from Fig. 9 in Ref. [2]. Triangles represent open-circuit voltages vs. Li^+/Li. In (b), T_N indicates an antiferromagnetic (AF) transition temperature, PM a paramagnetic phase, and SG a spin-glass-like phase.

cosine oscillation ($\exp(-\lambda t)\cos(\omega_\mu t + \phi)$) yields a delay of the initial phase (ϕ) by $\sim 40^\circ$, which is physically meaningless. We thus fit the ZF- μ^+SR spectrum by a zeroth-order Bessel function of the first kind ($J_0(\omega_\mu t)$), which describes the muon polarization evolution in an incommensurate (IC-) field distribution, and two exponentially relaxation functions [14]:

$$A_0 P_{ZF}(t) = A_{IC}\, e^{-\lambda_{IC} t} J_0(\omega_{IC} t) + A_{fast}\, e^{-\lambda_{fast} t} + A_{slow}\, e^{-\lambda_{slow} t}, \quad (1)$$

where A_0 is the empirical maximum muon decay asymmetry, A_{IC}, A_{fast}, and A_{slow} the asymmetries associated with the three signals, and λ_{IC}, λ_{fast}, and λ_{slow} are their relaxation rate. As T decreases from T_N^{mid}, f_{IC} ($\equiv \omega_{IC}/2\pi$) increases rapidly with decreasing the slope (df_{IC}/dT), and finally reaches around 30 MHz at 1.8 K, as expected for the order parameter of the AF transition. Considering the "1/3 tail" component due to a polycrystalline sample, the normalized A_{IC} suggests that almost whole sample is in the IC state below 35 K. It should be noted here that the ZF- μ^+SR spectrum of $LiNi_{3/4}Co_{1/4}O_2$ exhibits a spin-glass-like disordered magnetism below $\sim$ 10 K [15], altough the spin concentration in the MeO_2 (Me = metal) plane is the same to that in $Li_{0.75}NiO_2$, i.e., Ni^{3+} ions are magnetic with $S = 1/2$ ($t_{2g}^6 e_g^1$), while both Ni^{4+} and Co^{3+} ions non-magnetic with $S = 0$ (t_{2g}^6).

The oscillatory signal is also observed for the Li_xNiO_2 samples with $0.6 \leq x$, suggesting the formation of static AF order. Although the AF structure is not fully clarified at present, A-type AF order—i.e., FM in the plane but AF between the plane, is most reasonable to explain the results of χ and μ^+SR measurements, as in the case for $NaNiO_2$ [16]. On the other hand, a spin-glass-like disordered magnetism appears for the $x \leq 0.5$ samples at low T.

Finally, we draw a schematic magnetic phase diagram of Li_xNiO_2 (see Fig. 5). A dome-shaped AF phase region is found to exist in the x range between 1 and ~ 0.55, whereas the SG-like phase appears at $0.1 \leq x \leq 0.55$. Note that the χ measurements provide no information on the change in magnetic nature of Li_xNiO_2 with x. Although past work revealed the possibility to detect the change in physical/structural properties of Li_xNiO_2 during the charge reaction via. ^{7}Li NMR and χ measurements [17], the present result clearly demonstrates that not χ but μ^+SR measurements are most suitable for such purpose. Although the correlation between solid-state electrochemistry and magnetism of Li_xNiO_2 is currently unclear, we expect that further structural and physical analyses on Li_xNiO_2 especially at low-T provide a clear insight on the magnetic nature of lithium insertion materials in relation to electrochemical reactivity.

Acknowledgements

This work was performed at the Swiss Muon Source, Paul Scherrer Institut, Villigen, Switzerland. J. S. and Y. I. are partially supported by the KEK-MSL Inter-University Program for Oversea Muon Facilities. We thank the staff of PSI for help with the μ^+SR experiments. We also appreciate S. Kohno of OCU for preparation of $LiNiO_2$ and Y. Kondo of TCRDL for ICP-AES analysis. This work is also supported by Grant-in-Aid for Scientific Research (B), 1934107, MEXT, Japan.

References

[1] J.R. Dahn, U. von Sacken, C.A. Michal, Solid State Ionics 44 (1990) 87–97.
[2] T. Ohzuku, A. Ueda, M. Nagayama, J. Electrochem. Soc. 140 (1993) 1862–1870.
[3] J.B. Goodenough, D.G. Wickham, W.J. Croft, J. Phys. Chem. Solids 5 (1958) 107–116.
[4] L.D. Dyer, B.S. Borie, G.P. Smith Jr., J. Am. Chem. Soc. 76 (1954) 1499–1503.
[5] A. Rougier, C. Delmas, Solid State Commun. 94 (1995) 123–127.
[6] J.P. Peres, F. Weill, C. Delmas, Solid State Ionics 116 (1999) 19–27.
[7] G.M. Kalvius, D.R. Noakes, O. Hartmann, in: K.A. Gschneidner, L. Eyring, and G.H. Lander, et al. (Eds.), Handbook on the Physics and Chemistry of Rare Earths, vol. 32, North-Holland, Amsterdam, 2001, pp. 55–451, and references cited therein.
[8] A. Schenck, Muon Spin Rotation Spectroscopy Principles and Applications in Solid State Physics, Adam Hilger, Bristol (1985).
[9] K. Mukai, J. Sugiyama, Y. Ikedo, H. Nozaki, K. Simomura, K. Nishiyama, K. Ariyoshi, T. Ohzuku, J. Power Sources 174 (2007) 711–715.
[10] K. Mukai, Y. Ikedo, H. Nozaki, J. Sugiyama, K. Nishiyama, D. Andreica, A. Amato, P.L. Russo, E.J. Ansaldo, J.H. Brewer, K.H. Chow, K. Ariyoshi, T. Ohzuku, Phys. Rev. Lett. 99 (2007) 087601.
[11] A. Rougier, C. Delmas, G. Chouteau, J. Phys. Chem Solids 57 (1996) 1101–1103.
[12] E. Chappel, M.D. Núñez-Regueiro, S. de Brion, G. Choutea, Phys. Rev. B 66 (2002) 132412.
[13] J.N. Reimers, J.R. Dahn, J.E. Greedan, C.V. Stager, G. Liu, I. Davidson, U. von Sacken, J. Solid State Chem. 102 (1993) 542–552.
[14] J. Sugiyama, K. Mukai, Y. Ikedo, P.L. Russo, H. Nozaki, D. Andreica, A. Amato, K. Ariyoshi, T. Ohzuku, Phys. Rev. B, 78 (2008) 144412.
[15] K. Mukai, J. Sugiyama, Y. Ikedo, E.J. Ansaldo, G.D. Morris, K. Ariyoshi, T. Ohzuku, J. Power Sources 174 (2007) 843–846.
[16] M.J. Lewis, B.D. Gaulin, L. Filion, C. Kalin, A.J. Berlinsky, H.A. Dabkowsks, Y. Qiu, J.R.D. Copley, Phys. Rev. B 72 (2005) 014408.
[17] C. Chazel, M. Ménétrier, L. Croguennec, C. Delmas, Inorg. Chem. 45 (2006) 1184–1191.